Originally published as:

Impulsive feedback control of birhythmicity: Theory and experiment

Debabrata Biswas, Tanmoy Banerjee and Jürgen Kurths

View Online   Export Citation   CrossMark

ARTICLES YOU MAY BE INTERESTED IN

Impulsive feedback control of birhythmicity: Theory and experiment

View Online   Export Citation   CrossMark

Debabrata Biswas,[1,a)] (iD) Tanmoy Banerjee,[2] (iD) and Jürgen Kurths[3,4] (iD)

AFFILIATIONS

[1] Department of Physics, Bankura University, Bankura 722 155, West Bengal, India
[2] Chaos and Complex Systems Research Laboratory, Department of Physics, University of Burdwan, Burdwan 713 104,
West Bengal, India
[3] Potsdam Institute for Climate Impact Research, Telegraphenberg, D-14415 Potsdam, Germany
[4] Institute of Physics, Humboldt University Berlin, D-12489 Berlin, Germany

[a)] Author to whom correspondence should be addressed: debbisrs@gmail.com

ABSTRACT

We study the dynamic control of birhythmicity under an impulsive feedback control scheme where the feedback is made ON for a certain rather small period of time and for the rest of the time, it is kept OFF. We show that, depending on the *height* and *width* of the feedback pulse, the system can be brought to any of the desired limit cycles of the original birhythmic oscillation. We derive a rigorous analytical condition of controlling birhythmicity using the harmonic decomposition and energy balance methods. The efficacy of the control scheme is investigated through numerical analysis in the parameter space. We demonstrate the robustness of the control scheme in a birhythmic electronic circuit where the presence of noise and parameter fluctuations are inevitable. Finally, we demonstrate the applicability of the control scheme in controlling birhythmicity in diverse engineering and biochemical systems and processes, such as an energy harvesting system, a glycolysis process, and a p53-mdm2 network.

Published under an exclusive license by AIP Publishing. https://doi.org/10.1063/5.0089616

Birhythmicity is a potential variant of multistability exhibiting the coexistence of two stable limit cycles with different amplitudes and frequencies separated by an unstable limit cycle. The birhythmicity is perilous for many physical systems, whereas it is obvious and desirable in most biological systems. Hence, the control of birhythmicity deserves much attention. The control of multistability is a well studied topic, but surprisingly the control of birhythmicity is not. In this paper, we study and establish the efficacy of our impulsive feedback control scheme on controlling birhythmicity. The main advantage of the proposed scheme is that the control is required for a minimal period of time and then it may be switched off. We theoretically explore the control scheme and numerically establish the generality of the scheme. We demonstrate that the scheme is robust enough to work in a practical electronic circuit experiment in the presence of noise and fluctuations.

I. INTRODUCTION

Birhythmicity is a phenomenon where two stable limit cycles coexist separated by an unstable limit cycle in between them.[1,2] It is a potential variant of the ever prevailing multistability,[3] which arises in diverse fields of sciences including physics,[4,5] chemistry,[6] and biology.[7–9] The term "birhythmicity" was first introduced by Decroly and Goldbeter.[10] Since then, birhythmicity has been found in a energy harvesting system,[4] a Q-switched CO_2 laser,[11] a Josephson junction,[12] optoelectronics,[13] chemistry,[14–18] and biology (enzymatic reactions and glycolytic oscillators[6–8]). Most of the biochemical oscillators are birhythmic in nature[19,20] (see the recent review by Goldbeter and Yan[20] and references therein). In living systems, birhythmicity helps us to maintain biochemical processes to the environmental variations.[14] As examples of biochemical processes, we may suggest the following: intracellular Ca^{2+} oscillations,[2] glycolytic oscillators and enzymatic reactions,[6–8,21] the basic protein module that controls the proliferation of abnormal cells in mammals modeled by the birhythmic oscillations in the p53-Mdm2 network,[22,23] birhythmic oscillations generated in Adenosine Diphosphate (ADP) activated allosteric enzyme phosphofructokinage (PFK) due to the complex regulatory properties of it and finally feedback from ADP to Adenosine Triphosphase (ATP),[6] the circadian oscillation in period (PER) and timeless (TIM) proteins in Drosophila,[24] receptor

desensitization for the cyclic AMP signaling system of the slime mold *Dictyostelium discoideum*,[25] and oscillatory generation of cyclic adenosine monophosphate (CAMP) during the aggregation of the same.[26] Birhythmicity may be undesirable in many man-made systems[4,12] while it is desirable in others. This fact justifies the necessity and importance of controlling birhythmicity.

Although there exist several control schemes for bistable systems consisting of oscillatory and stable steady states,[27,28] control of birhythmicity is relatively a less explored topic (see the review on multistability by Pisarchik and Feudel[3]). Only a few control techniques are proposed and studied for birhythmicity. Ghosh *et al.*[29] employed a time-delayed feedback control of birhythmicity. Sevilla-Escoboza *et al.*[30] proposed that the application of harmonic modulation along with a positive feedback can control multistability and bring the system from coexisting chaotic and periodic attractors to a monostable one. Recently, Biswas *et al.*[31–33] showed that birhythmicity can be controlled by self-feedback or low-pass filtering and the system may be brought to any desired oscillating state. The switching between one limit cycle to another using an external pulse was reported in birhythmic[19] and trirhythmic[7,34,35] systems years ago. In those studies, the success of the control depends largely on the phase matching between the external perturbation and the limit cycles to be controlled.

In this paper, we study a more general and efficient control scheme that employs an impulsive feedback for controlling birhythmicity. In this control scheme, the feedback is made ON only for a certain period of time and then it is kept at an OFF state. Thus, unlike the previous control techniques, here the control needs not to be present all the time, and, therefore, the scheme remains noninvasive in the long run. Control through impulsive coupling is an important scheme and has been widely used to control the synchronization of chaos.[36–38] The intermittent control has been used for synchronization in Ref. 39 and for the selection of chaotic multistable attractors in Ref. 40. The impulsive control has been employed in the chemotherapy treatment of tumors, where the drug is used periodically with a proper amount and frequency.[41] Recently, Ref. 42 considered the transient temporal feedback with a step function to control coexisting chaotic attractors occupying different regions of phase space.

We establish the efficacy of the impulsive control scheme by carrying out an extensive theoretical analysis through the application of the harmonic decomposition technique and energy balance method. An extensive numerical analysis is performed to explore the effect of the width and height of the impulse on the control scenario. A prototypical birhythmic oscillator is constructed in an electronic circuit and the proposed control scheme is applied in the circuit to study the effectiveness of the scheme in the presence of parameter mismatch, noise, fluctuations, etc. Finally, we apply the control technique to control three real systems from diverse fields of physics and biology: (i) the energy harvesting system,[4] (ii) the glycolysis model (modified Goldbeter–Decroly model),[6,7] and (iii) the p53-Mdm2 network (OAK model).[22] The scheme is able to control the birhythmicity in all these systems. This proves the generality of the impulsive control scheme.

The paper is organized as follows: Sec. II discusses the birhythmic van der Pol oscillator. Section III describes the impulsive self-feedback control scheme. Section IV gives the analytical results
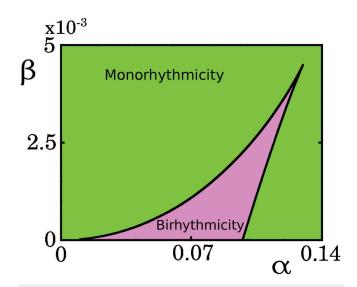

FIG. 1. Two-parameter bifurcation diagram of (1) in the $\alpha - \beta$ space for $\mu = 0.1$. The solid curves represent the saddle-node bifurcation of limit cycle (SNLC).

of the birhythmic van der Pol oscillator with the proposed coupling scheme. The numerical investigations are summarized in Sec. V. The experimental results are shown in Sec. VI. The efficacy of the present scheme is investigated in Appendixes A–C for the energy harvesting system, the glycolysis model, and the OAK model, respectively. Section VII concludes the outcome of the whole study.

II. THE BIRHYTHMIC VAN DER POL OSCILLATOR

The birhythmic van der Pol (vdP) oscillator is given by the following equation:[31,43,44]

$$\ddot{x} - \mu f(x)\dot{x} + x = 0, \tag{1}$$

where $x \in \mathcal{R}, f(x) = 1 - x^2 + \alpha x^4 - \beta x^6$ is the nonlinear function, and $\mu > 0, \alpha > 0, \beta > 0$ are parameters that determine the nonlinear damping.

The harmonic decomposition method considering $x(t) = A \cos \omega t$ leads to the following amplitude equation:[45]

$$\frac{5\beta}{64}A^6 - \frac{\alpha}{8}A^4 + \frac{1}{4}A^2 - 1 = 0, \tag{2}$$

which does not depend on the parameter μ and represents the generic form of the codimension-2 bifurcation. The birhythmicity emerges from the saddle-node bifurcation of limit cycle (SNLC). Figure 1 demonstrates the boundary between the bi- and monorhythmicity in the $\alpha - \beta$ parameter space (plotted using XPPAUT[46]).
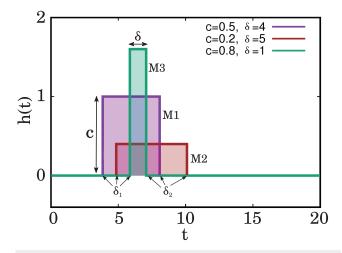
FIG. 2. Impulse function $h(t)$ [Eq. (4)]. The parameters controlling $h(t)$ are the height (c) and the width $((\delta_2 - \delta_1) = \delta)$. "M1": $c = 0.5$, $\delta = 4$, "M2": $c = 0.2$, $\delta = 5$, and "M3": $c = 0.8$, $\delta = 1$.

III. THE IMPULSIVE SELF-FEEDBACK CONTROL SCHEME

The birhythmic vdP oscillator with the impulsive feedback control is given by the following equation:

$$\ddot{x} - \mu f(x)\dot{x} + x = G(x, \dot{x}, t; p). \qquad (3)$$

Here, $G(x, \dot{x}, t; p)$ represents the control term given by $G(x, \dot{x}, t; p) = -dh(t)\dot{x}$, where d is the self-feedback strength. For $d > 0$, there is positive feedback and for $d < 0$ the feedback is negative; $d = 0$ represents the case of no feedback or uncontrolled system. $h(t)$ is an impulse function as follows:

$$h(t) = c\left[\text{sign}(t - \delta_1) - \text{sign}(t - \delta_2)\right], \qquad (4)$$

where c is the *height* of the impulse and $(\delta_2 - \delta_1) = \delta$ $(\delta_2 > \delta_1)$ is the *width* of the impulse. The "sign" function is given in the following:

$$\text{sign}(t - \zeta) = \begin{cases} 1 & \text{for} \quad t > \zeta, \\ -1 & \text{for} \quad t < \zeta, \end{cases} \qquad (5)$$

where $\zeta \in \mathcal{R}^+$. Figure 2 shows the form of the impulse for different sets of c and δ. It may be noted that the self-feedback is ON for a small time equal to the width of the impulse and after that, the self-feedback becomes OFF.

IV. ANALYSIS

We apply the harmonic decomposition method to understand the underlying dynamics of the controlled system (3). For this, we assume the approximate solution of Eq. (3) as

$$x(t) = A\cos\omega t. \qquad (6)$$

Substituting Eq. (6) into Eq. (3), we get the following equation:

$$\left(1 - \omega^2\right) A\cos\omega t$$

$$= \mu\omega\left(-1 + \frac{1}{4}A^2 - \frac{\alpha}{8}A^4 + \frac{5\beta}{64}A^6\right)A\sin\omega t$$

$$+ d\omega ch(t)A\sin\omega t$$

$$+ \mu\omega\left(\frac{1}{4}A^2 - \frac{3\alpha}{16}A^4 + \frac{9\beta}{64}A^6\right)A\sin 3\omega t$$

$$- \mu\omega\left(\frac{\alpha}{16}A^4 - \frac{5\beta}{64}A^6\right)A\sin 5\omega t$$

$$+ \mu\omega\frac{\beta A^6}{64}A\sin 7\omega t. \qquad (7)$$

The higher harmonics may be considered as forcing terms, which diminish with increasing harmonics. Thus, we can ignore them[47] and the above equation reads

$$\left(1 - \omega^2\right) A\cos\omega t$$

$$= \mu\omega\left(-1 + \frac{1}{4}A^2 - \frac{\alpha}{8}A^4 + \frac{5\beta}{64}A^6\right)A\sin\omega t$$

$$+ d\omega h(t)A\sin\omega t + \mathcal{H}, \qquad (8)$$

where $\mathcal{H}$ denotes the higher harmonic terms.

Equation (8) refers to the following frequency and amplitude equations, respectively,

$$1 - \omega^2 = 0 \qquad (9)$$

and

$$\mu\left(1 - \frac{1}{4}A^2 + \frac{\alpha}{8}A^4 - \frac{5\beta}{64}A^6\right) - dch(t) = 0. \qquad (10)$$

It may be noted that Eq. (10) reduces to Eq. (2) when the impulse is OFF (i.e, for any of the following: $d = 0$, $h(t) = 0$, or $c = 0$). Also, the system is independent of μ for the uncontrolled case. The frequency in the harmonic limit reduces to $\omega = 1$. Three limit cycles (two stable, one unstable) are the results of the three roots of the amplitude equation. To get an idea of the amplitude of the limit cycles, we analyze the stability of the system using the energy balance method.[48] The solution of Eq. (3) for $\mu = 0$ and $d = 0$ is given by

$$x(t) = A\cos(t + \phi), \qquad (11)$$

where ϕ is the initial phase that may be considered as $\phi = 0$ for convenience. The period of the circle in the phase plane is 2π. Thus, the harmonic solution becomes

$$x(t) \simeq A\cos(t). \qquad (12)$$

The change in energy ΔE in one period $0 \leq t \leq T(= 2\pi)$ is found by considering the term $\left(\mu F(x) - dh(t)\dot{x}\right)$ as the external

forcing term. Thus, the change in energy is given as

$$\Delta E = E(T) - E(0)$$

$$= \int_0^T \left(\mu F(x) - dh(t)\dot{x} \right) \dot{x} dt. \tag{13}$$

For a periodic solution (limit cycle), one gets $\Delta E = 0$. Thus, Eq. (13) on substitution of Eq. (12) yields

$$f(A^2) \equiv \pi \left(1 - \frac{1}{4}A^2 + \frac{\alpha}{8}A^4 - \frac{5\beta}{64}A^6 \right) \mu$$

$$+ cd \left(B_1 + B_2 - \frac{1}{2}(B_3 - B_4) \right) = 0, \tag{14}$$

where $B_1 = \Theta(\delta_1, \delta_2)(\delta_1 - \cos \delta_1 \sin \delta_1) + \Theta(\delta_1 - 2\pi, \delta_2)(2\pi - \delta_1 + \cos \delta_1 \sin \delta_1)$; $B_2 = \Theta(2\pi - \delta_1)\Theta(\delta_1)\Theta(\delta_2)(-\delta_2 + \cos \delta_2 \sin \delta_2 + \Theta(\delta_2 - 2\pi)(-2\pi + \delta_2 - \cos \delta_2 \sin \delta_2))$; $B_3 = \Theta(2\pi - \delta_1) \times (\Theta(-\delta_1) - 1)(-\Theta(\delta_1 - 2\pi)\Theta(\delta_2 - 2\pi)[4\pi - 2\delta_2 + \Theta(\delta_2 - \delta_1) \times (2\delta_2 - 2\delta_1 + \sin 2\delta_1 - \sin 2\delta_2) + \sin 2\delta_2] - \Theta(2\pi - \delta_1)\Theta(\delta_2 - \delta_1) \times [2\delta_2 - 2\delta_1 + \sin 2\delta_1 - \sin 2\delta_2 + \Theta(\delta_2 - 2\pi)(4\pi - 2\delta_2 + \sin 2\delta_2)])$; and $B_4 = \Theta(2\pi - \delta_2)(\Theta(-\delta_2) - 1))(-\Theta(2\pi - \delta_2)\Theta(\delta_1 - \delta_2) \times [2\delta_1 - 2\delta_2 - \sin 2\delta_1 + \Theta(\delta_1 - 2\pi)(4\pi - 2\delta_1 + \sin 2\delta_1) + \sin 2\delta_2] - \Theta(\delta_1 - 2\pi)\Theta(\delta_2 - 2\pi)[4\pi - 2\delta_1 + \sin 2\delta_1 + \Theta(\delta_1 - \delta_2)(2\delta_1 - 2\delta_2 - \sin 2\delta_1 + \sin 2\delta_2)])$. Here, $\Theta(u)$ is the "Heaviside Theta" function,

$$\Theta(u, v) = \begin{cases} 1 & \text{for} \quad \{u, v\} > 0, \\ 0 & \text{for} \quad \{u, v\} < 0. \end{cases} \tag{15}$$

We can determine the number of limit cycles by solving Eq. (14). The stability of the limit cycles is determined by the slope of the curve $f(A^2)$ (with A^2) obtained from Eq. (14) at the point of zero crossing. Hence, the condition of a stable limit cycle reads

$$\left. \frac{d\Delta E(A)}{dA} \right|_{LC} < 0. \tag{16}$$

To have an idea on the limit cycles and their stability, we plot Eq. (14) vs A^2 (Fig. 3). The roots of Eq. (3) are determined through the zero-crossing points of the curve. The stable LCs correspond to those, where the curve has a negative slope at the point of its zero crossings (shown in black filled circles in Fig. 3) and the unstable LC corresponds to the positive slope of the curve at the zero crossing (shown by the hollow circle). For the present case, we consider the following parameters: $\mu = 0.1$, $\alpha = 0.114$, $\beta = 0.003$, $c = 0.3$, and $\delta > 0 (= 50)$. In the figure, the broken green line shows the case for $d = -0.1$. It has only one solution, which represents a large amplitude limit cycle and the LC is a stable one owing to the negative slope at the zero-crossing point. The situation of birhythmic oscillation is shown by the solid blue line for $d = 0$. Here, one can see the existence of two stable LCs (negative slope) separated by an unstable LC (positive slope). For $d = 0.05$, the system has only one LC with a small amplitude. The case is shown in the figure with the broken red line.

V. NUMERICAL RESULTS

To explore the effect of impulsive coupling, we investigate system (3) numerically. We take $\alpha = 0.114$, $\beta = 0.003$ to keep the
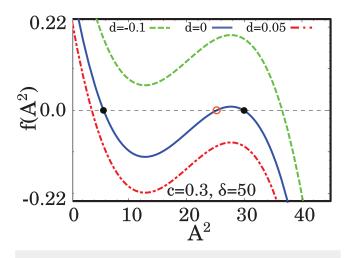

FIG. 3. Plot of $f(A^2) - A^2$ for the parameter set $\mu = 0.1$, $\alpha = 0.114$, $\beta = 0.003$, $\delta > 0 (=50)$, and $c = 0.3$ for different values of the control parameter d. The broken green (lighter) line shows the monorhythmic oscillation with large amplitude LC for $d = -0.1$. The broken red (light) line denotes the monorhythmic oscillations with small LC for $d = 0.05$ and the solid line indicates the birhythmic case for $d = 0$. Black filled circles represent the stable LC and hollow circle represents the unstable LC.

uncontrolled system ($d = 0$) in the birhythmic zone. The time series and phase plane plots are shown in Fig. 4. Figure 4(a) presents the time series for $d = 0$, which depicts the presence of two LCs of different amplitudes and frequencies. The thick red line in the time series shows the control signal $h(t)$ associated with the system (here, in the uncontrolled case, it is zero). We take the initial condition (IC) $\mathcal{I}_S \equiv (x(0), \dot{x}(0)) = (0.1, 0)$ to get the small amplitude LC and show this with the red line in Fig. 4, and for the large amplitude LC, we consider $\mathcal{I}_L \equiv (x(0), \dot{x}(0)) = (7, 0)$, which is shown by the green line in Fig. 4. Throughout the numerical investigations, we chose these values of initial conditions. We take the initial conditions separately to generate either small LC or large LC and then plot them in the same graph. The control $h(t)$ (solid red line) is nonzero for the duration of δ and then becomes zero. The nonzero portion is highlighted by the gray zone in the time series. The phase plane plots for $d = 0$ are shown in Fig. 4(b). Here also, one can notice the presence of two distinct limit cycles. Next, we consider $d = 0.3$ and the parameters controlling the impulse are given as: height $c = 0.5$, $\delta_1 = 200$, and $\delta_2 = 250$, i.e., the pulse width of the control is $\delta = 50$. As the control is ON the system oscillates with a small amplitude LC for both ICs. Now, if the control is switched OFF, the system remains in this small amplitude LC. Therefore, the control for a certain period of time is enough to select a desired limit cycle. This scenario is demonstrated through the time series in Fig. 4(c) and the corresponding phase plane plot in Fig. 4(d). It is interesting to note that in the beginning of the control pulse, at first both the LCs (large and small) decay into a transient amplitude death state and then eventually settle in to the intrinsic small amplitude LC.

Now, we fix $d = -0.3$; the other parameters remain the same as before. Here, as the control is made ON, the system oscillates with a large LC. The scenario is shown in Figs. 4(e) and 4(f). Here, it may
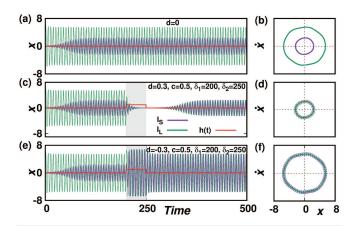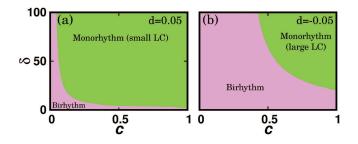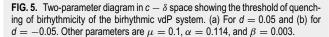
FIG. 4. Time series and phase plane plots for birhythmic vdP oscillator (3) along with the control pulse $h(t)$. (a) and (b) Birhythmic oscillation for $d = 0$, (c) and (d) monorhythmic oscillation with smaller amplitude LC for $d = 0.3$, and (e) and (f) monorhythmic oscillation with larger amplitude LC for $d = -0.3$. The initial conditions used are: $\mathcal{I}_S \equiv (x(0), \dot{x}(0)) = (0.1, 0)$ (violet line) and $\mathcal{I}_L \equiv (x(0), \dot{x}(0)) = (7, 0)$ (green line). The gray zone indicates the control ON zone. The phase plane plots are drawn for $t \geq 490$. Other parameters are: $\mu = 0.1$, $\alpha = 0.114$, $\beta = 0.003$, $c = 0.5$, $\delta_1 = 200$, and $\delta_2 = 250$, i.e., $\delta = 50 \approx 8T$.

be noted that before settling into the large LC, both LCs (small and large) jump to a LC whose amplitude is even larger than the large amplitude LC.

Next, we explore the efficacy of the control scheme in the parameter space. The present scheme has three control parameters, namely, the control strength d, the "height" of the impulse c, and the "width" of the impulse δ. At first, we investigate the effect of "height" c and "width" δ on the system by fixing the control strength d. For this, we fix $d = 0.05$ and investigate the threshold where a single LC emerged. The two-parameter ($c - \delta$) plot distinguishing these two zones is shown in Fig. 5(a). From the figure, it becomes clear that for moderate values of the "height" (c), the required "width" (δ) of the impulse function is very small to quench the birhythmicity. Next, we fix $d = -0.05$ to achieve a large amplitude LC: the plot in the $c - \delta$ space is shown in Fig. 5(b). Here also, we can see that one can select a desired LC beyond a boundary in the $c - \delta$ space. It is noteworthy

that the threshold of δ in this case is larger than in the previous case, i.e., the $d = 0.05$ case [Fig. 5(a)]. Energetically, this may be attributed to the fact that one requires more energy to bring the system to a large amplitude LC.

Next, we investigate the system in the $d - c$ parameter space for a fixed pulse width δ (we take $\delta = 10$). The scenario is shown in Fig. 6. From the figure, we can infer that for $d < 0$, one requires larger values of c to quench birhythmicity and to force the system to oscillate with large amplitude LC. For $d > 0$, the values of c are less to bring the system to oscillate with small amplitude LC. Finally, we demonstrate the results in the $d - \delta$ space for a constant "height" of the impulse (we take $c = 0.5$) in Fig. 7. In this case also, we see that the requirement of the threshold value of δ is larger for the large amplitude LC (i.e., $d < 0$) compared to the small amplitude LC (i.e., $d > 0$). At this point, it should be noted that after the feedback is turned off, the two stable limit cycles would still be possible. However, once a desired LC is reached, it remains there even after the control pulse is made OFF.
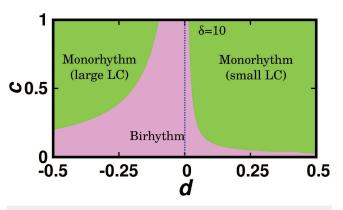

FIG. 6. Two-parameter diagram in $c - d$ space showing the threshold of quenching of birhythmicity for $\delta = 10$. Other parameters are same as Fig. 5.

FIG. 5. Two-parameter diagram in $c - \delta$ space showing the threshold of quenching of birhythmicity of the birhythmic vdP system. (a) For $d = 0.05$ and (b) for $d = -0.05$. Other parameters are $\mu = 0.1$, $\alpha = 0.114$, and $\beta = 0.003$.
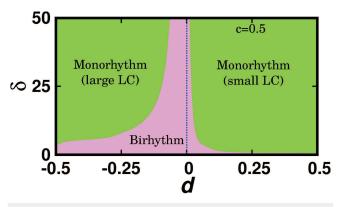

FIG. 7. Two-parameter diagram in $d - \delta$ space showing the threshold of quenching of birhythmicity for $c = 0.5$. Other parameters are the same as Fig. 5.
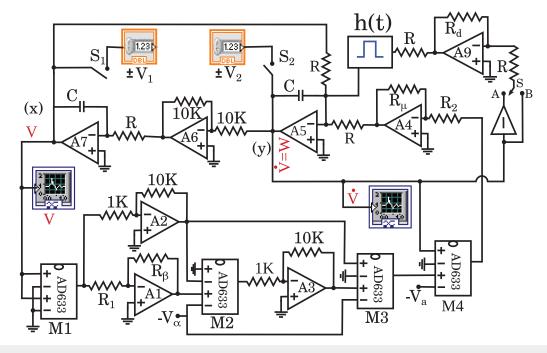
FIG. 8. The experimental circuit compatible to be controlled and acquired by Data Acquisition System (DAQ). For description and parameter values, see text.

Therefore, we can infer that, with the proper choice of control strength d and impulse parameters (c and δ), we can control birhythmicity and make the system oscillate to any one of the desired LCs. Further, all the results suggest that to bring the system to the large amplitude LC from its birhythmic state, the value of the impulse height and width (i.e., the pulse energy) has to be larger than that for a small amplitude LC. The generality of the control scheme is further explored in diverse man-made and biochemical processes. We consider a birhythmic energy harvesting system,[4] Decroly–Goldbeter model of glycolysis,[6,7] and p53:mdm2 network model[22] and apply the impulsive control scheme. In all cases, we found that a feedback in the form of a short pulse is capable of controlling birhythmicity (detailed results are given in Appendixes A–C). Therefore, we can conclude that the impulsive control scheme is general enough to control birhythmicity in physical and biological systems.

VI. EXPERIMENT

We design the birhythmic van der Pol oscillator in an electronic circuit with the impulsive self-feedback control given in Eq. (3). The detailed circuit is shown in Fig. 8. A portion of the self-feedback (W) is fed back to the integrator through a gain element (A9) and through a switching system [$h(t)$] in the circuit. The switch [$h(t)$] is realized with relay and microcontroller arrangement. The switch is in the ON state for a chosen time and then made OFF. Here, we use multiplier chips M1–M4 (AD633JN) and TL074 JFET opamps (A1–A9). The voltage equation of the circuit reads

$$RC\frac{dV}{dt} = W, \tag{17a}$$

$$RC\frac{dW}{dt} = \frac{R_\mu}{100R_2}\left[V_a - V^2\left(V_a - V^2\left(V_\alpha - \frac{R_\beta}{R_1}V^2\right)\right)\right]W$$
$$- V - \frac{R_d}{R}h(t)W, \tag{17b}$$

The above equation is made dimensionless by the following substitutions: $t = \frac{t}{RC}$, $x = \frac{V}{V_{sat}}$, $y = \frac{W}{V_{sat}}$, $\frac{R_\mu}{100R_2} = \mu$, $\frac{R_d}{R} = dc$, $V_a = a$ V, $V_\alpha = \alpha'$ V, and $\frac{R_\beta}{R_1} = \beta$; with these, Eq. (17) is reduced to Eq. (3). Real time data are acquired using Data Acquisition System (DAQ) (Model: NI USB-6351) with LabView interface.[49] The initial conditions of the circuit are controlled using a two-channel relay and a microcontroller (Arduino Uno).[50] Owing to the virtual ground of the opamps in the integrator (A5, A7), the capacitors (C) are initially charged to the desired voltage levels which are fed externally from the DAQ. These initial charges of the capacitors act as the initial conditions in the circuit when the relays are off. The impulsive self-feedback is realized by the relay-microelectronic arrangement. The relay is ON for a certain period of time that acts as the impulse ($h(t)$) in the system. This relay is also controlled by an Arduino Uno.

For the experiment, we use the following circuit elements: $R_\mu = 423\,\Omega$, $R_\beta = 1.14\,\mathrm{k\Omega}$, $C = 0.1\,\mu\mathrm{F}$, $V_\alpha = \alpha' = -1.185$ V, $V_a = a = -257.3$ mV, $R_1 = 1\,\mathrm{k\Omega}$, and $R_2 = R = 10\,\mathrm{k\Omega}$. We fix the initial conditions in the circuit as follows: for large amplitude LC $\mathcal{I}_L \equiv (V_1, V_2) = (4.1V, 0V)$ and for the small amplitude LC $\mathcal{I}_S \equiv (V_1, V_2) = (0.1V, 0V)$. When there is no control, i.e., $R_d = 0$ or the impulse is OFF [i.e., $h(t) = 0$]. In the experiment, only one set of initial conditions is used at a time. We acquire the real time data in the computer for the large and small amplitude LC separately owing
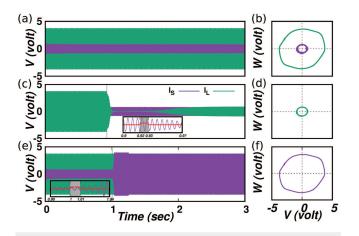
FIG. 9. The experimental time series and phase plane plots obtained by Data Acquisition System (DAQ). (a) and (b) $R_d = 0\,\Omega$: birhythmic oscillations; (c) and (d) $R_d = 1.06\,\text{k}\Omega$ (positive d, connecting "S" to "A"): transition from large amplitude LC to small amplitude LC (only the LC for $\mathcal{I}_L$ is shown); and (e) and (f) $R_d = 1.06\,\text{k}\Omega$ (negative d, connecting "S" to "B"): transition from small amplitude LC to large amplitude LC (only the LC for $\mathcal{I}_S$ is shown). The phase plane plots are drawn for $t \geq 2.8\,\text{s}$. The initial conditions are $\mathcal{I}_L \equiv (V_1, V_2) = (4.1V, 0V)$ for large amplitude LC and $\mathcal{I}_S \equiv (V_1, V_2) = (0.1V, 0V)$ for small amplitude LC. For other resistance and capacitance values, see text.

to the ICs $\mathcal{I}_L$ and $\mathcal{I}_S$, respectively, and plot them in the same diagram to show the presence of birhythmicity in the circuit. The time series and phase plane plots are shown in Figs. 9(a) and 9(b). Both plots show the occurrence of a large LC and a small LC in the circuit. Now we apply the impulsive control. The value of d is controlled by the potentiometer R_d. A positive value of d can be achieved by connecting the switch "S" to the point "A" in the circuit (Fig. 8). A negative d is obtained by connecting "S" to "B." First, we consider $d > 0$ and fix $R_d = 1.06\,\text{k}\Omega$. Now, we feed IC $\mathcal{I}_L$ in the circuit from DAQ. When the system starts oscillating in the large LC we apply the impulsive self-feedback for a period of $\delta = 0.01\text{s}$ (i.e., $\delta \approx 2\,\text{T}$). The system jumps from large amplitude LC to the small amplitude LC [see Figs. 9(c) and 9(d)]. The scenario is similar to that obtained in numerical investigations in Figs. 4(c) and 4(d). Next, we want to examine the situation for $d < 0$. We feed the system with the IC $\mathcal{I}_S$ (targeting the small LC). We use the previous value of d, i.e., $R_d = 1.06\,\text{k}\Omega$. When the impulsive feedback is given for $\delta = 0.01\text{s}$, the system eventually enters the large amplitude LC from the small one. The scenario is shown in Figs. 9(e) and 9(f). This particular situation is in good qualitative agreement with that shown in Figs. 4(e) and 4(f). Thus, the impulsive self-feedback can control birhythmicity in real electronic circuit where noise, fluctuations, and parameter mismatch are inevitable, and, thus, the scheme is robust.

VII. CONCLUSION

The paper reports the control of birhythmicity through an impulsive feedback control mechanism. The main essence of this particular control lies in the fact that the control is ON for a certain small period of time and then it becomes OFF, but the system is being controlled within that period and oscillates with the desired

limit cycle. The prominent merit of the present scheme is that for most of the time, it remains noninvasive and, thus, does not affect the inherent dynamics of the system. We have analyzed the system through harmonic decomposition and energy balance methods and obtained the required conditions for the control. Apart from the birhythmic van der Pol oscillator, we verify the effectiveness of the control scheme on an energy harvesting system, the Decroly–Goldbeter model of glycolysis, and the p53:mdm2 network model (Appendixes A–C). In all cases, it has been found that the control scheme can bring the system to a desired limit cycle. Finally, we have designed a prototypical birhythmic system, namely, the birhythmic van der Pol oscillator, in a hardware level electronic circuit and applied the control to the system. In the electronic circuit, which is a real system, despite the presence of parameter mismatch, noise, fluctuations, etc., the scheme is robust and efficient enough to control birhythmicity. Therefore, we believe that this study has potential applications in the field of control of birhythmicity in several biochemical and mechanical processes as well as in other fields of natural sciences.

AUTHOR DECLARATIONS
Conflict of Interest

The authors have no conflicts to disclose.

DATA AVAILABILITY

The data that support the findings of this study are available from the corresponding author upon reasonable request.

APPENDIX A: BIRHYTHMIC ENERGY HARVESTING SYSTEM UNDER IMPULSIVE SELF-FEEDBACK CONTROL

We consider the birhythmic energy harvesting system,[4] which produces electrical energy from ambient wind energy. The arrangement in the energy harvesting system possesses a cantilever attached to piezoelectric patches, which works under the transverse wind flow. The model has the following mathematical form:

$$\ddot{y} + \mu F(\dot{y}) + \Omega_0^2 y = \eta_0 v - dh(t)\dot{y}, \tag{A1a}$$

$$\dot{v} + \gamma v = -\eta_1 \dot{y}, \tag{A1b}$$

where $F(\dot{y}) = \left(-\dot{y} + \dot{y}^3/3 - \alpha \dot{y}^5/5 + \beta \dot{y}^7/7\right)$ is the nonlinear function and the impulsive control term is given by $-dh(t)\dot{y}$. For the present case, we consider the following parameters: $\mu = 0.1$, $\alpha = 0.144$, $\beta = 0.005$, $\Omega_0 = 1$, $\eta_0 = 0.1$, $\eta_1 = 0.25$, and $\gamma = 0.2$. Also, the following initial conditions are used: $\mathcal{I}_S$
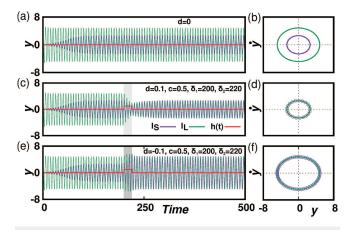
FIG. 10. Time series and phase plane plots of birhythmic energy harvesting system. (a) and (b) Birhythmic oscillation for $d = 0$, (c) and (d) monorhythmic oscillation with smaller amplitude LC for $d = 0.1$; (e) and (f) monorhythmic oscillation with larger amplitude LC for $d = -0.1$. The phase plane plots are drawn for $t \geq 490$. Other parameters are: $\mu = 0.1$, $\alpha = 0.144$, $\beta = 0.005$, $\Omega_0 = 1$, $\eta_0 = 0.1$, $\eta_1 = 0.25$, $\gamma = 0.2$, $c = 0.5$, $\delta_1 = 200$, and $\delta_2 = 220$ (i.e., $\delta = 20 \approx 4T$).
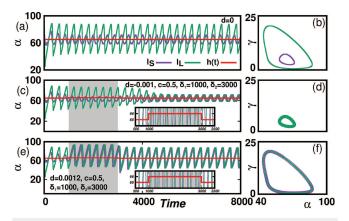

FIG. 11. Time series and phase plane plots of the glycolysis model. (a) and (b) Birhythmic oscillation for $d = 0$; (c) and (d) monorhythmic oscillation with smaller amplitude LC for $d = -0.001$, (e) and (f) monorhythmic oscillation with larger amplitude LC for $d = 0.0012$. The phase plane plots are drawn for $t \geq 7600$. Other parameters are: $\nu = 0.225$, $q = 0.1$, $K_s = 0.06$, $L = 3.6 \times 10^6$, $\sigma = 10$, $\sigma_i = 1.3$, $n = 4$, $K = 10.0$, $c = 0.5$, $\delta_1 = 1000$, and $\delta_2 = 3000$ (i.e., $\delta = 2000 \approx 7T$).

$\equiv (y(0), \dot{y}(0), v(0)) = (0.1, 0, 0.3)$ (targeting the small amplitude LC) and $\mathcal{I}_L \equiv (y(0), \dot{y}(0), v(0)) = (7, 0, 0.3)$ (targeting the large amplitude LC). With these parameters, we apply the impulsive control. We fix the "height" $c = 0.5$ and "width" $\delta = 20$ ($\delta \approx 4T$). The outcomes of this control are shown in Fig. 10. The uncontrolled case, i.e., $d = 0$, is shown in Figs. 10(a) and 10(b). The time series [Fig. 10(a)] and the phase plane plot [Fig. 10(b)] depict that the system is birhythmic in nature. Next, we fix $d = 0.1$. In this case, the system oscillates with small amplitude LC after the control the applied [Figs. 10(c) and 10(d)]. The system is brought to the large amplitude LC by taking $d = -0.1$. The scenario is shown in Figs. 10(e) and 10(f).

APPENDIX B: THE GLYCOLYSIS MODEL: MODIFIED DECROLY–GOLDBETER MODEL

The glycolysis model (modified Decroly–Goldbeter model),[6,7] which is closely related to the glycolytic oscillation in yeast and muscle and the periodic synthesis of cAMP during the aggregation of the slime mold *Dictyostelium discoideum*.[25] According to Kar and Ray[6] the modified Decroly–Goldbeter model, which is a product-activated enzyme model, along with the impulsive control given by

$$\frac{d\alpha}{dt} = \mu - \sigma\phi(\alpha, \gamma) + \frac{\sigma_i \gamma^n}{K^n + \gamma^n}, \tag{B1a}$$

$$\frac{d\gamma}{dt} = q\sigma\phi(\alpha, \gamma) - K_s\gamma - \frac{q\sigma_i \gamma^n}{K^+ \gamma^n} - dh(t)\gamma, \tag{B1b}$$

with

$$\phi(\alpha, \gamma) = \frac{\alpha(1 + \alpha)(1 + \gamma)^2}{L + (1 + \alpha)^2(1 + \gamma)^2}, \tag{B2}$$

where α is the normalized substrate concentration and γ is the normalized product concentration. We apply the impulsive control $(-dh(t)\gamma)$ in the second equation. For the present case, consider the following parameter set: $\nu = 0.225$, $q = 0.1$, $K_s = 0.06$, $L = 3.6 \times 10^6$, $\sigma = 10$, $\sigma_i = 1.3$, $n = 4$, and $K = 10.0$. The following initial conditions are used: $\mathcal{I}_S \equiv (\alpha(0), \gamma(0)) = (80, 5)$ (targeting the small amplitude LC) and $\mathcal{I}_L \equiv (\alpha(0), \gamma(0)) = (100, 5)$ (targeting the large amplitude LC).

In the impulsive control, we apply the following parameters: "height" $c = 0.5$, $\delta_1 = 1000$ and $\delta_2 = 3000$, i.e., "width" $\delta = 2000$ (here we use $\delta \approx 7 T$). Here, we wishfully choose an arbitrary pulse width ($\sim 7 T$, where T is the time period of the LC to be controlled) for better visibility. We investigate numerically the time series and phase plane plots. The birhythmic case for no control, i.e., $d = 0$ is shown in Figs. 11(a) and 11(b). The solid red line shows the control, which is drawn with an offset of 65 to align it at the center with the time series. The monorhythmic oscillations with small amplitude LC are shown in Figs. 11(c) and 11(d) for $d = -0.001$. For $d = 0.0012$, the system shows the monorhythmicity with large amplitude oscillations [Figs. 11(e) and 11(f)].

APPENDIX C: THE p53:mdm2 NETWORK: OAK MODEL

Ouattara, Abou-Jaoudé, and Kaufman's differential model of the p53-Mdm2 network (or the OAK model) is a birhythmic model that gives the proliferation of abnormal cells by proteins in mammals.[22] It describes the interaction between p53, cytoplasmic Mdm2, and nuclear Mdm2. The mathematical model with the impulsive self-feedback control reads

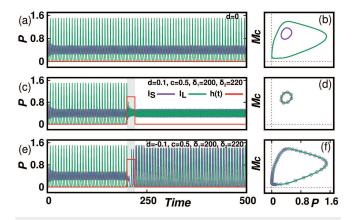$$\frac{dP}{dt} = k_P \frac{K_P}{K_P^n + M_n^n} - d_P P, \tag{C1a}$$

FIG. 12. Time series and phase plane plots of the p53-Mdm2 model. (a) and (b) Birhythmic oscillation for $d = 0$, (c) and (d) monorhythmic oscillation with smaller amplitude LC for $d = 0.1$, and (e) and (f) monorhythmic oscillation with larger amplitude LC for $d = -0.35$. The phase plane plots are drawn for $t \geq 490$. Other parameters are: $k_P = 5$, $K_P = 0.2$, $d_P = 2.5$, $k_{Mc} = 0.1$, $k'_{Mc} = 1.2$, $K_{MC} = 0.4$, $k_{in} = 0.45$, $k'_{in} = 0.4$, $K_{Mn} = 0.1$, $d_{Mc} = 0.6$, $V_r = 10$, $d_{Mn} = 1.9$, $n = 6$, $c = 0.5$, $\delta_1 = 200$, and $\delta_2 = 220$ (i.e., $\delta = 20$).

$$\frac{dMc}{dt} = k_{Mc} + k'_{Mc}\frac{P^n}{K^n_{Mc} + P^n} - \left(k_{in} - k'_{in}\frac{P^n}{K^n_{Mn} + P^n}\right)Mc$$
$$- d_{Mc}Mc - dh(t)Mc, \tag{C1b}$$

$$\frac{dMn}{dt} = V_r\left(k_{in}k'_{in}\frac{P^n}{K^n_{Mn}} + P^n\right), \tag{C1c}$$

where P, Mc, and Mn represent, respectively, the concentration of p53, cytoplasmic Mdm2, and nuclear Mdm2.

For numerical investigation, we apply the following parameter set: $k_P = 5$, $K_P = 0.2$, $d_P = 2.5$, $k_{Mc} = 0.1$, $k'_{Mc} = 1.2$, $K_{MC} = 0.4$, $k_{in} = 0.45$, $k'_{in} = 0.4$, $K_{Mn} = 0.1$, $d_Mc = 0.6$, $V_r = 10$, $d_{Mn} = 1.9$, and $n = 6$. The following initial conditions are used: $\mathcal{I}_S \equiv (P(0), Mc(0), Mn(0)) = (0.6, 0.3, 0.4)$ (targeting the small amplitude LC) and $\mathcal{I}_L \equiv (P(0), Mc(0), Mn(0)) = (3, 0.3, 0.2)$ (targeting the large amplitude LC). The parameters for the impulse are as follows: "height" $c = 0.5$ and "width" $\delta = 20$. The results of numerical investigations are shown in Fig. 12. The system shows birhythmic oscillations without the control, i.e., $d = 0$ [Figs. 12(a) and 12(b)]. The system exhibits monothythmicity with small amplitude LC for $d = 0.1$ as shown in Figs. 12(c) and 12(d). For $d = -0.35$, the system gives monorhythmicity with large amplitude oscillations as shown in Figs. 12(e) and 12(f).

Therefore, we may conclude that our control scheme is general enough to control birhythmicity in salient physical, biological, and man-made systems.

REFERENCES

[1] R. Lozi and S. Ushiki, Int. J. Bifurcation Chaos **1**, 923 (1991).
[2] A. N. Pisarchik, R. Jaimes-Reátegui, J. R. Villalobos-Salazar, J. H. García-López, and S. Boccaletti, Phys. Rev. Lett. **96**, 244102 (2006).
[3] A. N. Pisarchik and U. Feudel, Phys. Rep. **540**, 167 (2014).
[4] C. A. K. Kwuimy and C. Nataraj, in *Structural Nonlinear Dynamics and Diagnosis*, edited by M. Belhaq (Springer International Publishing, 2015), Vol. 168, pp. 97–123.
[5] D. Biswas and T. Banerjee, *Time-Delayed Chaotic Dynamical Systems* (Springer International Publishing, 2018).
[6] S. Kar and D. S. Ray, Europhys. Lett. **67**, 137 (2004).
[7] A. Goldbeter, *Biochemical Oscillations and Cellular Rythms. The Molecular Basis of Periodic and Chaotic Behavior* (Cambridge University Press, 1996).
[8] A. Goldbeter, Nature **420**, 238 (2002).
[9] R. Arumugam, T. Banerjee, and P. S. Dutta, Eur. Phys. J. ST **226**, 2145 (2017).
[10] O. Decroly and A. Goldbeter, Proc. Natl. Acad. Sci. U.S.A. **79**, 6917 (1982).
[11] F. Arecchi, R. Meucci, G. Puccioni, and J. Tredicce, Phys. Rev. Lett. **49**, 1217 (1982).
[12] R. Yamapi and G. Filatrella, Phys. Rev. E **89**, 052905 (2014).
[13] L. Weicker, T. Erneux, D. Rosin, and D. Gauthier, Phys. Rev. E **91**, 012910 (2015).
[14] M. Alamgir and I. Epstein, J. Am. Chem. Soc. **105**, 2500 (1983).
[15] D. Cohen and J. Keener, Chem. Eng. Sci. **31**, 115 (1976).
[16] M. Morita, K. Iwamoto, and M. Senō, Bull. Chem. Soc. Jpn. **61**, 3467 (1988).
[17] B. Johnson, J. Griffiths, and S. Scott, J. Chem. Soc. Faraday Trans. **87**, 523 (1991).
[18] T. Nagy, E. Verner, V. Gáspár, H. Kori, and I. Kiss, Chaos **25**, 064608 (2015).
[19] F. Morán and A. Goldbeter, Biophys. Chem. **20**, 149 (1984).
[20] A. Goldbeter and J. Yan, Interface Focus **12**, 192 (2022).
[21] S. Kar and D. S. Ray, Phys. Rev. Lett. **90**, 238102 (2003).
[22] W. Abou-Jaoudé, D. Ouattara, and M. Kaufman, J. Theor. Biol. **258**, 561 (2009).
[23] B. Vogelstein, D. Lane and A. J. Levine, Nature **408**, 307 (2000).
[24] J. C. Leloup and A. Goldbeter, J. Theor. Biol. **198**, 445 (1999).
[25] A. Goldbeter and J. L. Martiel, FEBS Lett. **191**, 149 (1985).
[26] J. L. Martiel and A. Goldbeter, Biophys. J. **52**, 807 (1987).
[27] A. N. Pisarchik and B. K. Goswami, Phys. Rev. Lett. **84**, 1423 (2000).
[28] A. N. Pisarchik, Phys. Rev. E **64**, 046203 (2001).
[29] P. Ghosh, S. Sen, S. S. Riaz, and D. S. Ray, Phys. Rev. E **83**, 036205 (2011).
[30] R. Sevilla-Escoboza, A. N. Pisarchik, R. Jaimes-Reátegui, and G. Huerta-Cuellar, Proc. R. Soc. London A **471**, 2015005 (2015).
[31] D. Biswas, T. Banerjee, and J. Kurths, Phys. Rev. E **94**, 042226 (2016).
[32] D. Biswas, T. Banerjee, and J. Kurths, Chaos **27**, 063110 (2017).
[33] D. Biswas, T. Banerjee, and J. Kurths, Phys. Rev. E **99**, 062210 (2019).
[34] O. Decroly and A. Goldbeter, C. R. Acad Sci. (Paris) Ser. II **298**, 779 (1984); available at https://www2.ulb.ac.be/sciences/utc/GOLDBETER/agoldbet.html.
[35] O. Decroly and A. Goldbeter, J. Theor. Biol. **113**, 649 (1985).
[36] T. Yang and L. Chua, IEEE Trans. Circ. Syst. I **44**, 976 (1997).
[37] Y.-W. Wang, Z.-H. Guan, and J.-W. Xiao, Chaos **14**, 199 (2004).
[38] C. Li, L. Chen, and K. Aihara, Chaos **18**, 023132 (2008).
[39] M. Schröder, M. Mannattil, D. Dutta, S. Chakraborty, and M. Timme, Phys. Rev. Lett. **115**, 054101 (2015).
[40] K. Yadav, N. Kamal, and M. D. Shrimali, Phys. Rev. E **95**, 042215 (2017).
[41] H.-P. Ren, Y. Yang, M. Baptista, and C. Grebogi, Phil. Trans. R. Soc. A **375**, 20160221 (2017).
[42] K. Yadav, A. Prasad, and M. D. Shrimali, Phys. Lett. A **382**, 2127 (2018).
[43] F. Kaiser and C. Eichwald, Int. J. Bifurcation Chaos **1**, 485 (2012).
[44] C. Eichwald and F. Kaiser, Int. J. Bifurcation Chaos **1**, 711 (2012).
[45] H. G. E. Kadji, J. B. C. Orou, R. Yamapi, and P. Woafo, Chaos Soliton. Fract. **32**, 862 (2007).
[46] B. Ermentrout, *Simulating, Analyzing, and Animating Dynamical Systems: A Guide to XPPAUT for Researchers and Students (Software, Environments, Tools)* (SIAM Press, 2002).
[47] D. W. Jordan and P. Smith, *Nonlinear Ordinary Differential Equations* (Oxford University Press, New York, 1999).
[48] R. Yamapi, B. R. N. Nbendjo, and H. G. E. Kadji, Int. J. Bifurcation Chaos **17**, 1343 (2011).
[49] N. Instruments, *Labview: Data Acquisition Basics Manual* (National Instruments, 1996).
[50] M. Banzi, *Getting Started with Arduino*, 2nd ed. (Make Books—Imprint of: O'Reilly Media, Sebastopol, CA, 2011).